Article

Nonlinear Electromagnetic Properties of Thinfilm Nanocomposites $(CoFeZr)_x(MgF_2)_{100-x}$

Evelina P. Domashevskaya [1,*], Sergey A. Ivkov [1], Pavel V. Seredin [1], Dmitry L. Goloshchapov [1], Konstantin A. Barkov [1], Stanislav V. Ryabtsev [1], Yrii G. Segal [1], Alexander V. Sitnikov [2] and Elena A. Ganshina [3]

[1] Department of Solid State Physics and Nanostructures, Voronezh State University, Voronezh 394018, Russia; ivkov@phys.vsu.ru (S.A.I.); ryabtsev@phys.vsu.ru (S.V.R.)

[2] Department of Solid State Physics, Voronezh State Technical University, 14 Moskovsky Ave., Voronezh 394026, Russia

[3] Department of Magnetism, Lomonosov Moscow State University, Moscow 119991, Russia

[*] Correspondence: ftt@phys.vsu.ru

Abstract: The aim of this work is a comprehensive study of the effect of variable atomic composition and structural-phase state of $(CoFeZr)_x(MgF_2)_{100-x}$ nanocomposites (NCs) on their nonlinear electronic and magnetic/magneto-optical properties. Micrometer-thick nanocomposite layers on the glass substrates were obtained by ion-beam sputtering of a composite target in the argon atmosphere in a wide range of compositions $x = 9$–51 at·%. The value of the resistive percolation threshold, $x_{per} = 34$ at·%, determined from the concentration dependencies of the electrical resistance of NCs, coincides with the beginning of nucleation of metallic nanocrystals CoFeZr in MgF_2 dielectric matrix. The absolute value of maximum magnetoresistance of NCs is 2.4% in a magnetic field of 5.5 kG at $x = 25$ at·%, up to the percolation threshold. Two maxima appear in the concentration dependencies of magneto-optical transversal Kerr effect, one of which, at $x = 34$ at·%, corresponds to the formation of CoFeZr alloy nanocrystals of a hexagonal structure, and the second one at $x = 45$ at·% corresponds to the phase transition of nanocrystals from a hexagonal to a cubic body-centered structure. The magnetic percolation threshold in $(CoFeZr)_x(MgF_2)_{100-x}$ system at $x_{fm} = 34$ at·%, with the appearance of a hysteresis loop and a coercive force of $H_c \approx 8$ Oe, coincides with the resistive percolation threshold $x_{per} = 34$ at·%. Concentration dependence of the coercive force showed that at low contents of metallic alloy $x < 30$ at·%, NCs are superparamagnetic ($H_c = 0$). With an increase of the alloy content, in the region of magnetic and resistive percolation thresholds, NCs exhibit a magnetically soft ferromagnetic character and do not change it far beyond the percolation threshold, with the maximum value of the coercive force $H_c < 30$ Oe.

Keywords: nanocomposites; nanocrystals; magnetoresistance; percolation threshold; magneto-optical properties; transversal Kerr effect; superparamagnetic; soft ferromagnetic

1. Introduction

Metal-dielectric magnetic nanocomposites (NCs) have a number of unique physical properties that are promising for their use in spintronics, information recording and storage technologies, shielding coatings, sensitive magnetic sensors, and other devices.

For the first time, the tunnel type of giant magnetoresistance (GMR) in metal-dielectric $Ni-SiO_2$ films was discovered in [1–3]. Later, the authors of [4] obtained sputtered Co-based CoAlO granular alloy thin films, which were characteristic in exhibiting GMR of about 8%, accompanying a large specific electrical resistivity of the order of 10^{-2} Ω·cm due to a weak tunnel conductance in the metal–nonmetal granular structure of this alloy. It was found [4] that GMR changes in a dependent matter on Co content and shows a maximum near the percolation threshold where transition from metallic conductance to the tunnel one takes place in Co-Al-O granular alloy thin films. In addition, superparamagnetic behavior in the

magnetic field and temperature dependencies of magnetization have been found for the GMR alloy films. The observations support the spin-dependent tunneling effect for this new GMR.

Next, the problem of the influence of the phase composition and atomic structure of metal-dielectric granular composites, which were realized in the process of self-organization during their preparation, on the electrical, magnetic, and magneto-optical properties became a challenging subject of intensive experimental and theoretical studies [5–10]. All of these properties of composites depend nonlinearly on the phase composition and atomic structure and, in particular, on the concentration of the magnetic metal phase, the shape and size of metal granules, and their distribution over the bulk of the sample. In this regard, electroresistive, magnetic, and magneto-optical (MO) studies, which are sensitive to the characteristic sizes, shapes, and topology of metal particles, are of considerable interest [5–11].

For granular composites, there is the concept of the percolation threshold x_{per}, i.e., a value of the concentration of the metal component, at which the final "conductive network" of contacting metal particles is formed in the entire volume of the sample. One can say that the percolation region is an intermediate state during the transition from electrically nonconductive to the electrically conductive state, where metal granules start coming into contact between each other. In this region, all the unique physical properties that are inherent in granular metal-dielectric composites are manifested to a greater extent [4,11].

Thus, in granular metal-dielectric composites, depending on the value of the volume fraction of the metal component x, two types of conductivity are possible. When this fraction is large, the metal granules come into contact and form a conductive network so that electrons can flow directly through the connected metal channels, and the composite exhibits metallic conductivity. When the volume fraction of the metal component is small, well below the percolation threshold, the granules of the metal are distributed as separate dispersed metal particles in the insulating matrix. The electrical conductivity in this state is determined by the hopping conductivity of electrons tunneling from one metal particle to another through the dielectric regions. Tunneling conductivity is retained up to x_c ($x_{per} > x > x_c$), where the metal-dielectric transition occurs. In this concentration range, unusual transport phenomena, such as the tunneling anomalous Hall effect and the logarithmic temperature dependence of the conductivity, were detected [12]. It has been experimentally established that, for a large number of granular metal-dielectric composites, the percolation threshold is close to the interval $x_{per} \approx 0.5$–0.6 [11].

The behavior of magnetic properties in ferromagnetic metal-insulator NCs is even more complex. In the region of low concentrations of the metal component $x < x_{per}$, NC exhibits superparamagnetic properties, while in the region of high metal concentrations $x > x_{per}$, it demonstrates ferromagnetic properties. Most often, the magnetic percolation threshold x_{fm} does not coincide with the transport one [13] and is usually less than x_{per} since the ferromagnetic order FM can arise without physical contact between the granules as a result of the exchange interaction. Therefore, x_{fm} can be defined as the concentration at which magnetization sharply increases, and a coercive force arises in nanocomposites.

The main methods for producing composite films are thermal, cathode, and ion-plasma sputtering. Each of these methods has its own advantages and disadvantages depending on the sputtered material and the purpose of using NC. Monograph [11] analyzes the existing methods for obtaining granular composites, and it is concluded that the most universal method is ion-plasma magnetron sputtering, when the separation of the condensing medium into two components (metal and dielectric) is carried out as a result of their self-organization in a single precipitation process. As a magnetic component of film composites, ferromagnetic metals Fe, Co, Ni, and their alloys are usually applied, which are often amorphized under additions of boron or zirconium. Most of the known metal-dielectric composite systems are obtained using oxide dielectrics SiO_2, Al_2O_3, MgO, TiO_2, ZrO_2. At the same time, due to oxygen presence in a condensing medium, a significant

oxidation of the surface of metal granules occurs, which affects the electrical, magnetic, and magneto-optical (MO) characteristics of the composites.

Recently, studies of composites with oxygen-free dielectrics have been realized. For example, in [14], when studying the magnetotransport properties of $(Fe_{51}Co_{49})_{32}(MgF_2)_{68}$ film with $Fe_{51}Co_{49}$ alloy distributed in MgF_2 dielectric matrix, a giant magnetoresistance of 13.3% at 10 kOe was found at room temperature. In [15], the frequency dependence of the tunnel-type magnetodielectric effect in $Co_x(MgF_2)_{1-x}$ superparamagnetic nanostructures was demonstrated with an exact change in x in the range from 0.06 to 0.2.

In [16,17], the electrical and magnetoresistive properties of $Co_x(MgF_2)_{100-x}$ thin films were studied in a wide range of metal phase concentrations ($14 \leq x$, at·% ≤ 62) in the initial state and after thermal annealing in vacuum. The percolation threshold for this system is set in the range $x = 30$–36 at·% Co. The magnetoresistive effect of the studied samples attained 7% in a field of 10 kOe at cobalt concentration $x = 25$ at·%. When samples are heated up to 250 °C in the composites containing cobalt, up to the percolation threshold, the magnitude of the magnetoresistance increases, while in composites above the percolation threshold it decreases. It has been found that the matrix of the MgF_2 system is resistant to thermal heating up to 250 °C. Raising the temperature to 350 °C leads to the disappearance of the magnetoresistive effect.

In [18,19], we studied in detail the features of the atomic structure, phase formation, and substructure of the same $Co_x(MgF_2)_{100-x}$ nanocomposites depending on the ratio of metal and dielectric components using X-ray diffraction (XRD), X-ray photoelectron spectroscopy (XPS), and infrared spectroscopy (IR). It was found that when the content of cobalt Co $x < 29$ at·%, metal is in the X-ray amorphous state in the form of clusters in the MgF_2 nanocrystalline matrix. With an increase in the cobalt content up to $x = 42$ at·% on a glass substrate, cobalt nanocrystals of hexagonal syngony, already in the amorphous dielectric matrix MgF_2, with the sizes of about 10 nm, are formed, predominantly oriented in the plane of the basis of the hexagonal lattice (001) α-Co.

Then, in [20], we studied the effect of atomic composition and the structural-phase state of $Co_x(MgF_2)_{100-x}$ nanocomposites on their nonlinear transport and magnetic/magneto-optical properties. It was shown that the beginning of Co nanocrystal formation coincides with the attainment of electric and magnetic percolation thresholds at x = 37 at·% and is accompanied by a transition from a superparamagnetic to a soft ferromagnetic state, which, under an increase in the metal content (x > 42 at·%), acquires a magnetic hardness with a coercive force of up to 95 Oe.

At the same time, we conducted a study of nanocomposites of a more complex atomic composition with a three-element magnetic alloy CoFeZr in the same oxygen-free dielectric matrix MgF_2 [21,22].

As a metallic component, we selected a three-element alloy $Co_{45}Fe_{45}Zr_{10}$, which previously showed the largest value of TMR in the SiO_2 matrix of the composites $(CoFeZr)_x(SiO2)_{1-x}$, even in comparison with Co and Fe in the same matrix [11]. The same applies to our choice of an oxygen-free dielectric MgF_2 as a matrix, in which metal granules Co and Fe showed the highest values of TMK compared to oxide matrices [11].

The studies of nanocomposites of variable composition $(CoFeZr)_x(MgF_2)_{100-x}$ by X-ray diffraction XRD, X-ray electron spectroscopy XPS, and infrared spectroscopy IR showed that the relative content of the CoFeZr metal alloy in the oxygen-free nanocomposite affects its atomic structure, substructure [21], conductivity and magneto-optical properties of the material in the most significant way [22].

The aim of this work is to show the influence of the atomic composition and structural-phase changes of $(CoFeZr)_x(MgF_2)_{100-x}$ nanocomposites on their nonlinear electronic and magnetic/magneto-optical properties.

To demonstrate this relationship to the fullest extent in this paper, we used some results of structural and magneto-optical studies of $(CoFeZr)_x(MgF_2)_{100-x}$ nanocomposites from our previous works [21,22] in the Sections 3.1 and 3.3. This is due to the fact that the Mössbauer spectra presented in this paper (Section 3.2) made it possible to explain the

softer magnetic properties of $(CoFeZr)_x(MgF2)_{100-x}$ NCs compared to the harder magnetic properties of $Co_x(MgF_2)_{100-x}$ NCs [20].

2. Materials and Methods

Composite films with a different content of metallic alloy CoFeZr in the MgF_2 dielectric matrix were obtained using an original ion-beam deposition setup described in [11]. The composite target consisted of the $Co_{45}Fe_{45}Zr_{10}$ amorphous metal alloy plate with an uneven and asymmetric placement of the dielectric MgF_2 inserts; as a result, the concentration gradient is formed in the sputtered material in a single cycle within the argon atmosphere at the operating pressure of $\sim 5 \times 10^{-4}$ Torr on glass substrates of a size of 50×40 mm [11,22]. Then, the substrate with the nanocomposite was cut into 10 strips with a width of 5 mm and a length of 40 mm; in each strip, the atomic composition of the nanocomposite, the relative content of alloy x (the sum of the concentrations of three metals), and the thickness of the composite layer were determined at least three to five points. Therefore, on the concentration dependencies of the electronic and magnetic properties of a nanocomposite of variable composition $(CoFeZr)_x(MgF2)_{100-x}$, discrete points denote the results of the corresponding measurements obtained for these 10 certified samples of a certain composition x and a certain thickness. The same 10 certified samples are presented in Tables 1–3.

Table 1. Parameters of the Mössbauer spectra of CoFeZr and FeF$_2$ phases in the composition of the sample $(CoFeZr)_{51}(MgF_2)_{49}$: S—magnetic sextet; D—paramagnetic doublet; Is—isomeric shift; Q—quadrupole splitting; H—effective magnetic field on α-Fe; G—line width; A—area of the component under the spectrum.

Sample $(CoFeZr)_{51}(MgF_2)_{49}$	Componente	Is, mm/c	Q, mm/c	H, кOe	G, mm/c	A, %	Phase Identification
(CoFeZr)	S	−0.08	0	339	0.7	82	α-Fe
(FeF$_2$)	D	0.85	1.92		0.77	18	FeF$_2$

Table 2. Concentration dependence of the electrical resistance of nanocomposites $(CoFeZr)_x(MgF_2)_{100-x}$ for 10 samples with different x.

CoFeZr, x, at·%	9	14	20	25	30	34	38	44	47	50
R, Ohm	4×10^9	4×10^7	1×10^6	3×10^4	6×10^2	110	45	12	11	6

Table 3. Concentration dependence of the total electric resistance R and capacitance C of the nanocomposites $(CoFeZr)_x(MgF_2)_{100-x}$.

x, at·%	R, Ohm	C, f
20	13×10^6	6×10^{-12}
25	25×10^4	4×10^{-12}
30	830	4×10^{-9}
34	136	1.2×10^{-9}
38	75	-
43	16	-
47	8	-
50	8	-

The phase composition of nanocomposites formed as a result of self-organization of two components, metallic and dielectric in different ratios, and was studied by X-ray diffraction (XRD) with DRON-4 diffractometer applying Co-Kα radiation in the step-by-step scanning mode (Russia) [20]. CoFeZr concentration in atomic % and thicknesses of film composites were determined using electron probe X-ray spectral microanalysis with an attachment to a JEOL JSM-6380LV (Japan) scanning electron microscope (Akishima-Shi, Tokyo, Japan); the error did not exceed 1.5% of the content of the measured element. The thicknesses of the investigated films of nanocomposites on glass substrates varied in the range of 0.9–3.4 µm, in accordance with an increase in the CoFeZr alloy content (*x*, at·%) in the range of *x* = 9–51 at·%.

The study of the magnetoresistive effect was carried out by direct measurement of the electrical resistance of the samples with a change in the external constant magnetic field using the four-probe method at an ECOPIA HMS-3000 (South Korea) setup. The device package included a certified magnetic attachment with a magnetic induction of B = 5.5 kG.

The impedance was measured by applying an alternative signal using an Elins Z-1500 J impedancemeter (Russia). The studies were carried out at room temperature in the frequency range from 1 MHz to 3 MHz. The amplitude of the alternating measuring signal did not exceed 100 mV. The measurement error did not exceed 5%. The analysis of the impedance spectra was carried out within the framework of the model of serially connected parallel equivalent circuits using the procedure for processing experimental data with modern software.

To study the magnetic properties of nanocomposites, we used an automated Lake Shore 7404 VSM vibrating magnetometer with a sensitivity of 10^{-5}–10^{-7} G·cm^3. Magneto-optical (MO) properties of the nanocomposites were studied in the geometry of the transversal Kerr effect (TKE) with an automated MO spectrometer in the incident light energy range E from 0.5 to 4 eV at room temperature [22]. The amplitude of the applied alternating magnetic field attained 3 kOe. The spectral, field, and concentration dependencies of the TKE were measured in the dynamic mode when the sample under study was in an alternating magnetic field. This method allowed for the use of a differential measurement scheme and an increase accuracy in measuring the relative light intensity to ~10^{-5}.

3. Results and Discussions

3.1. Structural-Phase Composition of Nanocomposites Depending on the Alloy Content in the Dielectric Matrix

In Figure 1, we reproduce the diffraction patterns of nanocomposite samples from our previous work [21] with a different alloy content *x* at·%, which is shown to the right of each diffraction pattern. For comparison, polycrystalline samples of cubic BCC iron α-Fe and hexagonal cobalt α-Co are presented on the two upper diffractograms, and the powder of tetragonal MgF2 is presented on the lower diffractogram.

Obtained in [21], XRD data shows that in the region of low concentrations (x $\leq$ 25 at·%), the metal alloy CoFeZr is in the X-ray amorphous state in the form of metal clusters distributed in MgF$_2$ nanocrystalline matrix, represented in diffraction patterns by two wide reflections (110) and (220).

The first phase transition in composites is the formation of a nanocrystalline phase based on the a-Co hexagonal lattice from the amorphous CoFeZr alloy, which occurs with an increase in the alloy content to x ~34% and corresponds to the percolation threshold. At the same time, the MgF$_2$ dielectric matrix makes an antibate transition from the nanocrystalline to the amorphous state, and instead of the most intense line (110) MgF$_2$, a wide gallo appears. It should be noted that, unlike metallic α-Co, the most intense of the three diffraction lines characteristic of α-Co in a nanocrystalline alloy at x = 34 is the line (100). This indicates the predominant orientation of hexagonal CoFeZr nanocrystals in the direction (100) of the amorphous MgF$_2$ matrix. The average size of nanocrystals is about 10 nm.
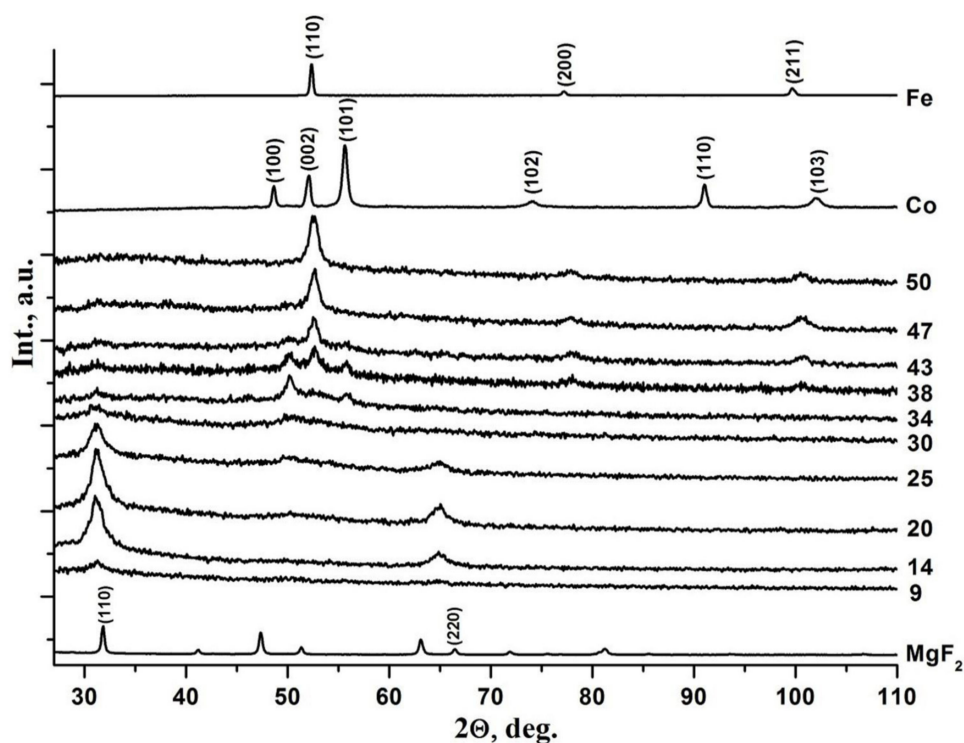
Figure 1. Diffractograms of nanocomposites with different compositions. $(CoFeZr)_x(MgF_2)_{100-x}$ on the glass substrates. Alloy CoFeZr content *x* (at·%) is shown to the right of each diffractogram.

However, already at x = 38, the middle of the three lines becomes the most intense, which gradually, with an increase in x = 47, remains the only diffraction line characteristic of the α-Fe crystal lattice. Thus, at the concentration of the alloy x = 47, the second phase transition of the nanocrystals of the CoFeZr alloy occurs from a hexagonal structure to a cubic volume-centered one, and their average sizes reach 20 nm.

Thus, as a result of self-organization under non-equilibrium conditions of ion-plasma sputtering at certain concentration ratios of the metal and dielectric components of nanocomposites, mutually inverse (antibate) phase transitions occur from the amorphous to the nanocrystalline state of the metal alloy, with an increase in its content in the composite and the reverse transition of the MgF_2 dielectric phase from the nanocrystalline to the amorphous state.

At the same time, XRD showed that MgF_2 nanocrystals of the dielectric matrix in the composites have slightly increased interplanar distances d_{110} and d_{220} compared to the reference microcrystalline MgF_2 [21]. In [21], we used two other methods of diagnosing the phase composition of materials with a complex atomic composition, XPS and IR spectroscopy, which could not unambiguously establish the cause of these changes.

3.2. Determination of Chemical Bonds of Iron Atoms in a Nanocomposite $(CoFeZr)_{51}(MgF_2)_{49}$ by the Nuclear Gamma Resonance Method of Mössbauer Spectroscopy

Since the increased values of the interplane distances d_{110} and d_{220} of the nanocrystals of the dielectric matrix of the MgF_2 were closer to the corresponding values in the iron and cobalt fluorides FeF_2 and CoF_2, which we had not previously detected by IR spectroscopy and XPS X-ray electron spectroscopy [21], we attempted to detect the interaction of iron atoms with fluorine by the Mössbauer nuclear spectroscopy.

Figure 2 shows two Mössbauer spectra: the calibration spectrum from α-Fe (left) and the spectrum from the sample $(CoFeZr)_{51}(MgF_2)_{49}$ with the maximum magnetic alloy content x = 51 at·% (right).

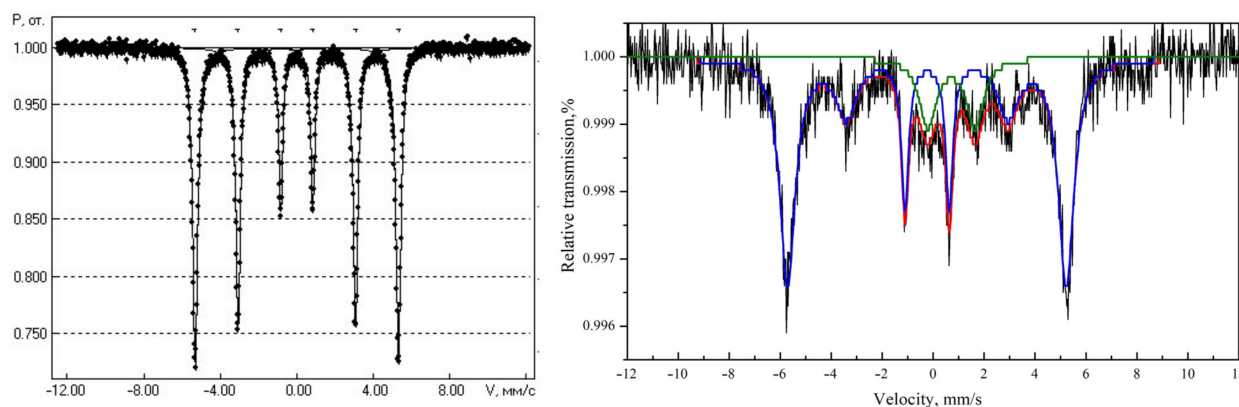**Figure 2.** Mössbauer spectra: Calibration α-Fe (**left**) and nanocomposite $(CoFeZr)_{51}(MgF_2)_{49}$ (**right**).

The total amount of accumulation of statistics in the Mössbauer spectrum from this sample was more than 500 h.

In the Mössbauer spectrum of the sample $(CoFeZr)_{51}(MgF_2)_{49}$, an intense magnetic sextet (hyperfine magnetic splitting) is isolated with parameters (Is = -0.08 mm/s, Q = 0 mm/s G = 0.70 mm/s, H = 339 kE) close to α-Fe (see left calibration spectrum in Figure 2), which we refer to as iron in the composition of nanocrystals of the CoFeZr alloy with the BCC structure α-Fe.

However, along with the magnetic sextet, the spectrum of the nanocomposite contains a paramagnetic quadrupole doublet related to iron fluoride FeF_2 with parameters (Is = -0.85 mm/s, Q = 1.92 mm/s). The ratio of the areas of these two spectra from the phases in the nanocomposite sample (magnetic alloy CoFeZr and paramagnetic phase FeF_2) is 82:18, with a total area of 100 for NC $(CoFeZr)_{51}(MgF_2)_{49}$ (Table 1).

Thus, the appearance of an additional doublet from the paramagnetic phase FeF_2 in the Mössbauer spectrum of the nanocomposite $(CoFeZr)_{51}(MgF_2)_{49}$ indicates that at the interfacial boundaries of nanocrystals of a magnetic alloy CoFeZr with a dielectric MgF_2, the boundary iron atoms interact with the fluorine atoms of the dielectric matrix to form the paramagnetic phase of iron fluoride FeF_2. This circumstance can significantly affect the magnetic properties of the studied nanocomposites.

3.3. Concentration Dependencies of Electrical Resistance and Magnetoresistance

Concentration dependence of the electrical resistance of nanocomposites $(CoFeZr)_x$ $(MgF_2)_{100-x}$ for 10 samples with different alloy content x (at·%) is shown in Figure 3a and in Table 3. This dependence of the resistivity of the studied nanocomposites is characterized by the nonlinear pattern of metal-dielectric composites behavior, when the electric transfer mechanism changes with variations in the relative content of metal and dielectric components [11,23–29].

Figure 3a and Table 3 shows that in the range of x = 9–25 at·%, the resistance of nanocomposites $(CoFeZr)_x$ $(MgF_2)_{100-x}$ falls by five orders of magnitude from 4×10^9 to 3×10^4, but remains characteristic of dielectrics. With a further increase in the alloy content from 35 to 50 at·%, the resistance of nanocomposites drops sharply to values characteristic of alloys and even some metals.

In the graph of the concentration dependence (Figure 3a), we draw two extrapolation lines with different angles of inclination. The range of intersection of these lines in the region (30–35 at·%) corresponds to the percolation threshold. Two straight lines on the concentration dependence indicate different current flow mechanisms before and after the percolation threshold along the high-resistance and low-resistance pathways. The obtained experimental data correlates well with the data for similar systems of composites with dielectrics of barium fluoride, calcium fluoride, and aluminum oxide [23–29].
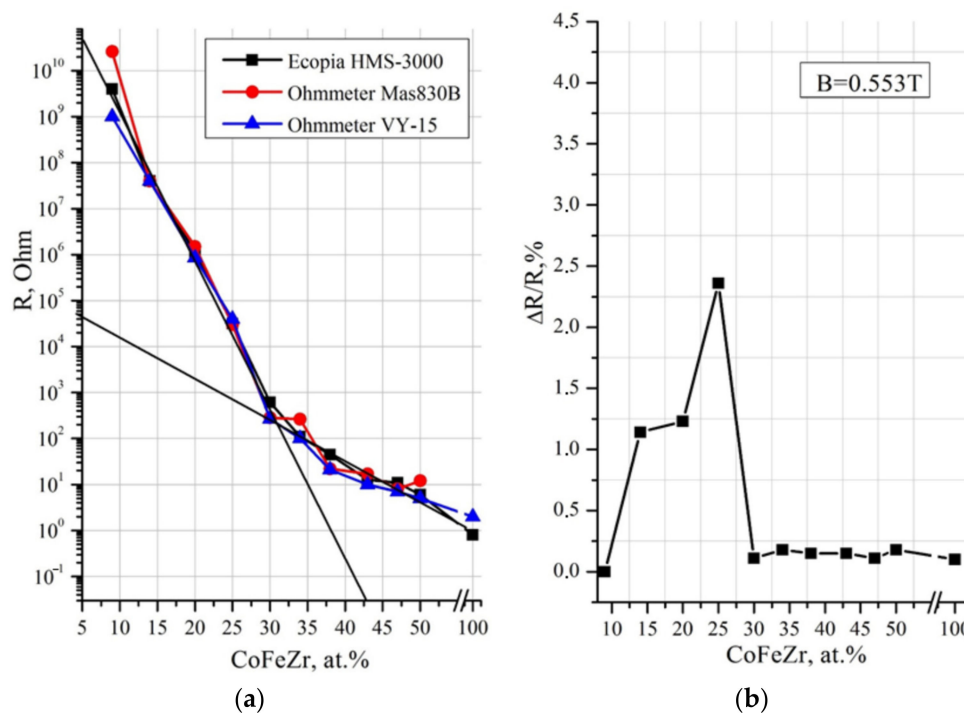
Figure 3. Concentration dependencies of electrical resistance (**a**) and magnetoresistance (**b**) of $(CoFeZr)_x(MgF_2)_{100-x}$ nanocomposites. The points on the curves correspond to samples with different values of x, which were measured.

The absolute values of the tunneling giant magnetic resistance (GMR) were determined in accordance with the expression:

$$\frac{\Delta R}{R(0)} = \frac{R(H) - R(0)}{R(0)} * 100\%,$$

where $R(H)$ is the resistance of the sample in the presence of an external magnetic field H, $R(0)$ is the resistance of the composite in the absence of an external magnetic field.

Figure 3b shows the concentration dependence of magnetoresistance for the samples of the system $(CoFeZr)_x(MgF_2)_{100-x}$. The resulting concentration dependence of magnetoresistance is extremely nonmonotonic. In the dielectric region of composites, small values of magnetoresistance are recorded far from the percolation threshold. With an increase relative to the content of the metal component in the range of 9 < x < 27, the GMR increases abruptly to the maximum value of $\Delta R/R(0) = 2.4\%$. With a further increase in the proportion of the metal component (x > 27 at·%), GMR is also sharply reduced.

The obtained concentration dependence of the magnetoresistive effect is fully consistent with the general model of tunneling magnetoresistance [25–30], according to which the number of electrons tunneling through the dielectric barrier increases with decreasing distance between neighboring alloy nanocrystals. Near the percolation threshold, the morphology of composites is such that the dielectric layer between the nanocrystals has a minimum thickness. The appearance of an exchange interaction between alloy nanocrystals/granules with decreasing distance follows from the analysis of Slonchevsky [30].

Thus, with an increase in the content of CoFeZr alloy in the nanocomposite, the average size of nanocrystals increases from 10 to 20 nm [21], and the distance between them decreases. This leads to the mechanical contact of neighboring nanocrystals and the formation of extended fractal-like metal clusters. As a result, the number of energy barriers decreases and the mechanism of electric transfer through the nanocomposite starts to change from tunneling to ohmic one (Table 2).

3.4. Capacitive/Inductive Nature of the Resistance of (CoFeZr)$_x$(MgF$_2$)$_{100-x}$ Nanocomposites According to Impedancemetry Data

One of the most accessible methods for studying electrophysical processes is impedance spectroscopy [31,32].

$$\text{Impedance is } Z = R - i\frac{1}{\omega C}$$

where $i = \sqrt{-1}$, ω is the cyclic frequency, C is the total capacitance of the composite. $Z' = R$ is the real resistance component, $Z'' = \frac{1}{\omega C}$ is the imaginary resistance component.

The hodograph of the impedance Z (impedance diagrams) is a graphical dependence of the imaginary component of the impedance Z'' on the real Z'.

For (CoFeZr)$_x$(MgF2)$_{100-x}$ nanocomposites, impedancemetry data in Figure 4 shows two different types of hodographs before percolation threshold and after the percolation threshold. On the hodograph for a nanocomposite with an alloy content up to the percolation threshold $x \geq 34$ at·%, a semicircle is observed, which corresponds to the typical behavior of the RC chain of metal clusters in a dielectric matrix [32]. At the percolation threshold $x \geq 35$ at·%, the hodograph takes the form of an inclined line, and then, as x increases beyond the percolation threshold, the hodographs become vertical lines, indicating the metallic nature with the ohmic character of conduction [32].
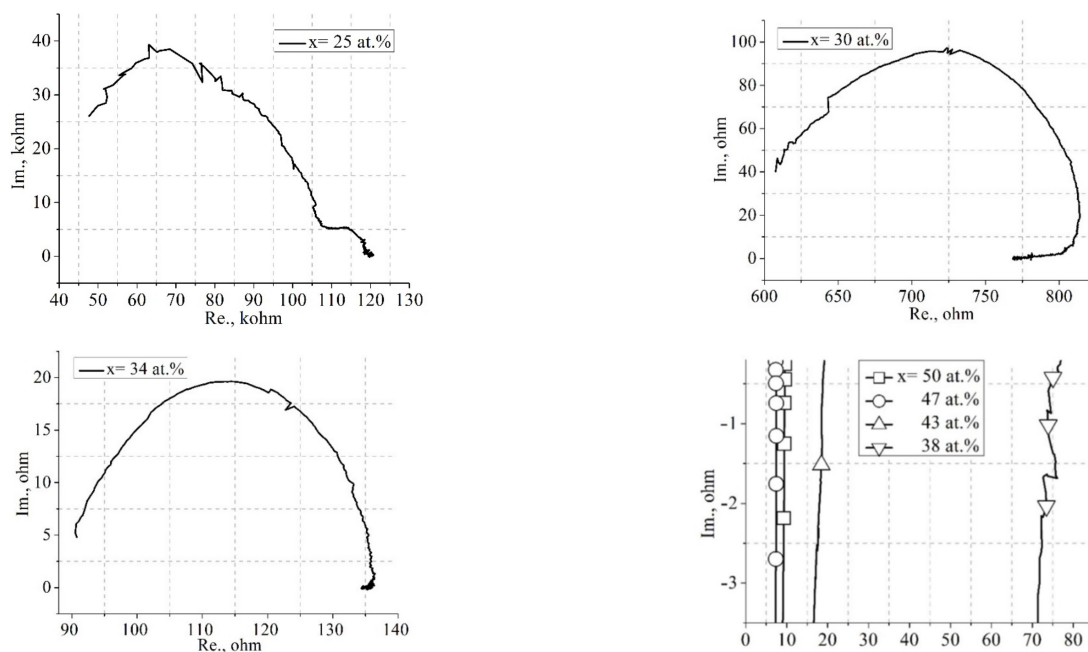

Figure 4. Impedance diagrams (hodographs) for nanocomposites (CoFeZr)$_x$(MgF$_2$)$_{100-x}$ of different compositions.

The resistance and capacitance of the nanocomposites, according to the impedancemetry data given in Table 3, show that the capacitance of the nanocomposites in the prepercolation region does not exceed several picofarads. Additionally, only in the region of the percolation threshold ($x_{per} = 34$ at·%), the capacitance increases by three orders of magnitude up to two nanofarads. This increase in capacitance value is due to the beginning of the formation of metallic nanocrystals and the remaining dielectric interlayers between them.

The presented data correlate well with the capacitive properties of a similar system (CoFeZr)$_x$(PZT)$_{100-x}$ from [33].

3.5. Magneto-Optical and Magnetic Properties of (CoFeZr)$_x$(MgF$_2$)$_{100-x}$ Nanocomposite

The magneto-optical Kerr effect in transversal geometry [6–9], transversal Kerr effect (TKE), consists of changing the intensity of linearly polarized light reflected by a sample

magnetized perpendicular to the plane of the incident light. The value and sign of TKE are defined as the ratio of the difference between the intensities of the light reflected by the sample in the magnetized (I) and demagnetized (I_0) states to the light intensity I_0:

$$\delta = I - I_0/I_0 = \Delta I/I_0$$

The absolute value of TKE depends on the amount of the metal phase in the composite. Its increase leads to an increase in the TKE modulus, which attains a maximum concentration corresponding to the percolation threshold.

Figure 5 from our previous work [22] shows the concentration dependencies of TKE for $(CoFeZr)_x(MgF_2)_{100-x}$ nanocomposites at three values of the incident light photon energy of E = 1.14 eV, 1.97 eV, and 3.17 eV. The concentration dependencies of TKE in the NC $(CoFeZr)_x(MgF_2)_{100-x}$ system showed two maxima, one of which, at $x = 30$–34 at·%, corresponded to the formation of hexagonal nanocrystals of the CoFeZr alloy and the second maximum at $x = 45$ at·% corresponded to the phase transition of the hexagonal structure to the cubic BCC structure α-Fe.
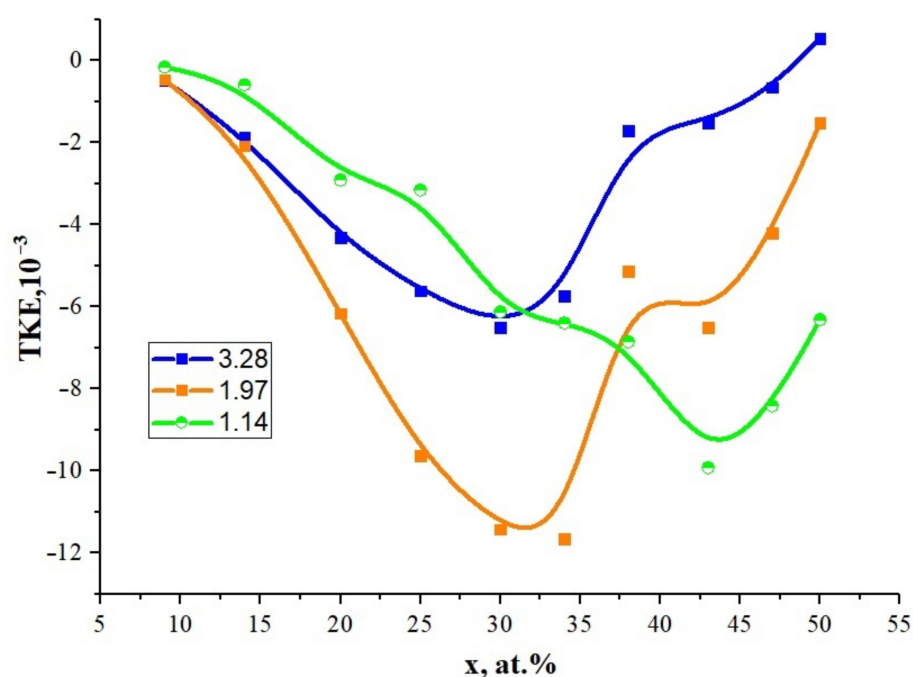

Figure 5. Concentration dependencies of transversal Kerr effect (TKE) for nanocomposites $(CoFeZr)_x(MgF_2)_{100-x}$ at different values of the incident light energy 1.14 eV (red curve), 1.97 eV (blue curve), and 3.17 eV (green curve). The points on the curves correspond to 10 samples with different values of x.

Thus, magneto-optical spectra respond to changes in the composition, atomic structure, and magnetic order of complex heterophase systems. It is in this effect that the quantum nature of light manifests itself, which is very sensitive to the spatial distribution of atoms in the alloy nanocrystals and the magnetic ordering associated with it.

The magnetic percolation threshold x_{fm} is defined as the concentration of the metal phase when the magnetization increases sharply and a coercive force arises in nanocomposites. Further, in Figure 6, we present the dependencies of magnetizations on the magnetic field arising parallel and perpendicular to the sample plane, which show the first appearance of a hysteresis loop with a coercive force $H_c \approx 18$ Oe in a $(CoFeZr)_{34}(MgF_2)_{66}$ sample for the alloy content $x = 34$ at·% corresponding to the formation of hexagonal CoFeZr nanocrystals.
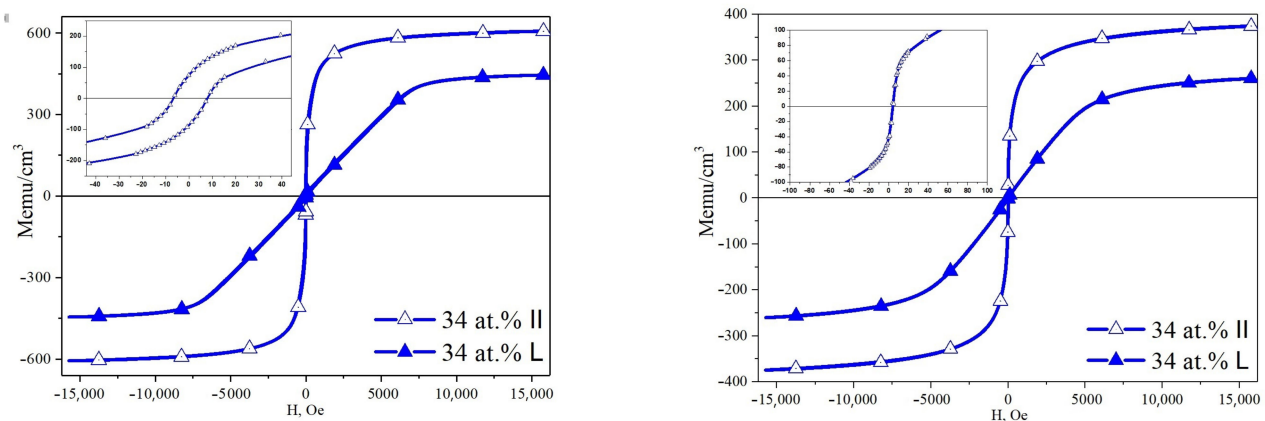
Figure 6. Appearance of hysteresis in the sample $(CoFeZr)_{34}(MgF_2)_{66}$ with $x = 34$ at·% and its absence in the sample $(CoFeZr)_{30}(MgF_2)_{70}$ with $x = 30$ at·%.

This means that the magnetic percolation threshold in the $(CoFeZr)_x(MgF_2)_{100-x}$ system at $x_{fm} = 34$ at·% coincides with the resistive percolation threshold $x_{per} = 34$ at·% due to the exchange interaction between electrons and spins of the formed hexagonal CoFeZr nanocrystals.

Figure 7 shows the dependence of coercive force H_c on the concentration of the metal component for nanocomposites $(CoFeZr)_x(MgF_2)_{100-x}$ on the glass. The measurements of the NC's magnetic properties with a vibration magnetometer showed that the value of the coercive force H_c in all of the nanocomposites at $x \leq 30$ at·% is equal to zero.
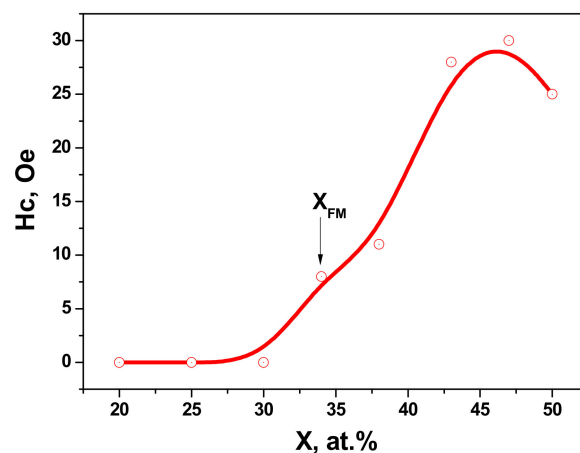

Figure 7. Concentration dependence of the coercive force H_c in $(CoFeZr)_x(MgF_2)_{100-x}$ nanocomposites. The points on the curves correspond to samples with different values of x, in which the coercive force was measured.

Thus, in the concentration region of $x \leq 30$ at·%, nanocomposites $(CoFeZr)_x(MgF_2)_{100-x}$ are superparamagnets, and the critical magnetic percolation threshold for this system is $x_{fm} = 34$ at·%. However, as the x value increases, hysteresis loops with non-zero H_c values appear in the samples.

According to the magnitude of the coercive force N_c, magnetic materials are divided into magnetically hard and magnetically soft. Materials with values of $N_c < 50$ Oe are magnetically soft, and materials with $N_c > 50$ Oe are magnetically hard. Based on this classification, the studied nanocomposites $(CoFeZr)_x(MgF_2)_{100-x}$ should be attributed to soft magnetic materials with a maximum value of $H_c < 30$ Oe (Figure 7).

It should be noted that the nanocomposites of the less complex composition $Co(MgF_2)_{100-x}$, which we have recently studied [20], containing one metallic cobalt in the same matrix,

exhibit more magnetic hardness at approximately the same cobalt concentrations, with a maximum coercive force of about 90Oe. Apparently, the decrease in magnetic order in NCs $(CoFeZr)_x(MgF_2)_{100-x}$ is influenced by the diamagnetic phase FeF_2 that we discovered at the interface of magnetic nanocrystals CoFeZr with a dielectric matrix MgF_2 by the Mössbauer spectroscopy.

4. Conclusions

Thus, the results of comprehensive studies of the structural-phase, electrical resistive, and electromagnetic properties of thin-film samples of heterogeneous metal-dielectric system $(CoFeZr)_x(MgF_2)_{100-x}$ with variable composition, obtained by ion-plasma sputtering on glass substrates, show that in a wide range of the studied compositions x = 9–51 at·%, nanocomposite consists of one X-ray amorphous phase and one nanocrystalline phase.

Which of the two components, metallic CoFeZr or dielectric MgF_2, forms nanocrystals in the composite depends on the relative alloy content x. At x < 34 at·%, the metal phase is X-ray amorphous and the MgF_2 dielectric matrix is nanocrystalline, while at x > 34 at·%, metallic alloy is formed in hexagonal nanocrystals and the dielectric matrix becomes X-ray amorphous. Starting from x = 43 at·%, the crystal structure of CoFeZr nanocrystals is rearranged into a cubic volume-centered phase based on α-Fe with a predominant orientation of (110), like that of α-Fe. The average size of CoFeZr alloy nanocrystals increases within 10–20 nm.

At the metal-insulator interfaces in $(CoFeZr)_x(MgF_2)_{100-x}$, the formation of Fe-F chemical bonds between iron and fluorine atoms with the formation of a paramagnetic FeF_2 phase by the Mössbauer spectroscopy was found.

The value of the percolation threshold of nanocomposites x_{per} = 34 at·%, determined from the concentration dependencies of the electrical resistance of nanocomposites, coincides with the beginning of the nucleation of metal CoFeZr hexagonal nanocrystals in the MgF_2 dielectric matrix.

The absolute value of the maximum negative magnetoresistance in the investigated NCs is 2.4% in the field of 5.5 kOe at the alloy concentration of x = 25 at·%, up to the percolation threshold.

The magnetic percolation threshold in the $(CoFeZr)_x(MgF_2)_{100-x}$ system occurs at x_{fm} = 34 at·%, with the appearance of a hysteresis loop and a coercive force Hc $\approx$ 18 Oe, coinciding with the resistive percolation threshold x_{per} = 34 at·% and with the beginning of the CoFeZr hexagonal nanocrystals nucleation.

In the concentration dependencies of the magneto-optical transversal Kerr effect in the $(CoFeZr)_x(MgF_2)_{100-x}$ NCs, two maxima appear, one of which corresponds to the formation of CoFeZr alloy nanocrystals of a hexagonal structure (x = 34 at·%), and the second maximum at x = 45 at·% corresponds to the phase transition of nanocrystals from a hexagonal structure to a cubic body-centered structure. It is in this effect that the quantum nature of light manifests itself, which is very sensitive to the spatial distribution of atoms in the alloy nanocrystals and the magnetic ordering associated with it.

Electric and magnetic percolation thresholds in $(CoFeZr)_x(MgF_2)_{100-x}$ NCs at x = 34 at·% coincides with the formation of CoFeZr nanocrystals. Below this value x < 34 at·%, nanocomposites exhibit superparamagnetic properties.

At large values of x > 34 at·%, $(CoFeZr)_x(MgF_2)_{100-x}$ NCs become magnetically soft materials and remain far beyond the percolation thresholds with the maximum value of the coercive force.

H_c < 30 Oe. Apparently, the decrease in magnetic order and soft ferromagnetic are influenced by the diamagnetic phase FeF_2 that we discovered at the interface of magnetic nanocrystals CoFeZr with a dielectric matrix MgF_2 by the Mössbauer spectroscopy.

Author Contributions: Conceptualization, E.P.D.; methodology, E.P.D., A.V.S. and E.A.G.; validation, E.A.G. and P.V.S.; formal analysis, E.P.D.; investigation, S.A.I., S.V.R., D.L.G. and Y.G.S.; writing—original draft preparation, E.P.D., S.A.I. and E.A.G.; writing—review and editing, E.P.D. and S.A.I.; supervision, E.P.D.; project administration, P.V.S.; E.P.D. and E.A.G. analyzed the data; S.A.I., P.V.S.,

References

1. Gittleman, J.L.; Goldstain, J.; Borowski, S. Magnetic Properties of Granular Nikel Films. *Phys. Rev. B.* **1972**, *5*, 3609–3621. [CrossRef]
2. Helman, J.S.; Abeles, B. Tunneling of Spin-Polarized Electrons and Magnetoresistance in Granular Ni Films. *Phys. Rev. Lett.* **1976**, *37*, 1429–1433. [CrossRef]
3. Abeles, B.; Sheng, P.; Coutts, M.D.; Arie, Y. Structural and electrical properties of granular metal films. *Adv. Phys.* **1975**, *24*, 407–461. [CrossRef]
4. Fujimori, H.; Mitani, S.; Ohnuma, S. Tunnel-type GMR in metal-nonmetal granular alloy thin films. *Mater. Sci. Eng. B* **1995**, *31*, 219–223. [CrossRef]
5. Zvezdin, A.K.; Kotov, V.A. *Modern Magnetooptics and Magnetooptical Materials*; Institute of Physics Publishing Ltd.: London, UK, 1997.
6. Gan'shina, E.; Granovsky, A.; Gushin, V.; Kuzmichev, M.; Podrugin, P.; Kravetz, A.; Shipil, E. Optical and Magneto-Optical Spectra of Magnetic Granular Alloys. *Physika A* **1997**, *241*, 45–51. [CrossRef]
7. Kravets, V.G.; Petford-Long, A.K.; Kravets, A.F. Optical and magneto-opticalproperties of $(CoFe)_x(HfO_21)_{1-x}$ magnetic granular films. *J. Appl. Phys.* **2000**, *87*, 1762–1768. [CrossRef]
8. Gan'shina, E.A.; Kim, C.G.; Kim, C.O.; Kochneva, M.Y.; Perov, N.Y.; Sheverdyaeva, P.A. Magnetostatic and magneto-optical properties of Co-based amorphous ribbons. *J. Magn. Magn. Mater.* **2002**, *239*, 484–486. [CrossRef]
9. Gan'shina, E.A.; Vashuk, M.V.; Vinogradov, A.N.; Granovskij, A.B.; Gushchin, V.S.; Shcherbak, P.N.; Kalinin, Y.E.; Sitnikov, A.V.; Kim, C.O.; Kim, C.G. Evolution of optical and magneto-optical properties in amorphous metal-dielectric nanocomposites. *J. Exp. Theor. Phys.* **2004**, *125*, 1172–1183. [CrossRef]
10. Buravtsova, V.E.; Guschin, V.S.; Kalinin, Y.E.; Kirov, S.; Lebedeva, E.; Phonghirun, S.; Sitnikov, A.; Syr'ev, N.; Trofimenko, I. Magnetooptical properties and FMR in granular nanocomposites $(Co_{84}Nb_{14}Ta_2)_x(SiO_2)_{100-x}$. *CEJP* **2004**, *2*, 566–578. [CrossRef]
11. Gridnev, S.A.; Kalinin, Y.E.; Sitnikov, A.V.; Stogney, O.V. *Nonlinear Phenomena in Nano—And Microheterogeneous Systems*; BINOM Knowledge Laboratory: Moscow, Russia, 2012; p. 352.
12. Rylkov, V.V.; Nikolaev, S.N.; Chernoglazov, K.Y.; Demin, V.A.; Sitnikov, A.V.; Presnyakov, M.Y.; Vasiliev, A.L.; Perov, N.S.; Vedeneev, A.S.; Kalinin, Y.E.; et al. Tunneling anomalous Hall effect in the nanogranular CoFeB–AlO films near metal-insulator transition. *Phys. Rev. B* **2017**, *95*, 144402. [CrossRef]
13. Bedanta, S.; Kleemann, W. Superparamagnetism. *J. Phys. D* **2009**, *42*, 013001. [CrossRef]
14. Kobayashi, N.; Ohnuma, S.; Masumoto, T.; Fujimori, H. (Fe–Co)–(Mg-fluoride) insulating nanogranular system with enhanced tunnel-type giant magnetoresistance. *J. Appl. Phys.* **2001**, *90*, 4159–4162. [CrossRef]
15. Cao, Y.; Umetsu, A.; Kobayashi, N.; Ohnuma, S.; Masumoto, H. Tunable frequency response of tunnel-type magneto-dielectric effect In Co_xMgF_2 granular films with different content of Co. *Appl. Phys. Lett.* **2017**, *111*, 122901. [CrossRef]
16. Tregubova, T.; Stognei, O.; Kirpan, V. Magnetotransport properties of $Co_x(MgF_2)_{100-x}$ oxygen-free nanocomposites. In *EPJ Web of Conferences; Moscow International Symposium on Magnetism*; EDP Sciences: Les Ulis, France, 2018; p. 01014. [CrossRef]
17. Tregubova, T.V.; Stogney, O.V.; Tregubov, I.M.; Kirpan, V.V. Electrical and magnetoresistive properties of oxygen-free composites Cox(MgF2)100-x. *Vestn. Voronezh State Tech. Univ.* **2017**, *13*, 122–127.
18. Domashevskaya, E.P.; Ivkov, S.A.; Sitnikov, A.V.; Stogney, O.V.; Kozakov, A.T.; Nikolsky, A.V. Formation of nanocrystals of a metal or dielectric component depending on their relative content in $Co_x(MgF_2)_{1-x}$ composites. *Solid State Phys.* **2019**, *61*, 211–219. [CrossRef]
19. Domashevskaya, E.P.; Ivkov, S.A.; Stogney, O.V.; Sitnikov, A.V. Mutual influence of the relative content of the metallic and dielectric component on the phase composition and substructure of nanocomposites $Co_x(MgF_2)_{1-x}$. In Proceedings of the 8th International Conference on Nanotechnology and Materials Science, Amsterdam, The Netherlands, 24–26 April 2019; p. 81.
20. Ivkov, S.A.; Barkov, K.A.; Domashevskaya, E.P.; Ganshina, E.A.; Goloshchapov, D.L.; Ryabtsev, S.V.; Sitnikov, A.V.; Seredin, P.V. Nonlinear Transport and Magnetic/Magneto-Optical Properties of $Co_x(MgF_2)_{100-x}$ Nanostructures. *Appl. Sci.* **2023**, *13*, 2992. [CrossRef]

21. Domashevskaya, E.P.; Ivkov, S.A.; Sitnikov, A.V.; Stogney, O.V.; Kozakov, A.T.; Nikolsky, A.V.; Barkov, K.A.; Builov, N.S. The features of CoFeZr alloy nanocrystals formation in film composites of $(CoFeZr)_x(MgF_2)_{100-x}$. *J. Alloys Compd.* **2021**, *870*, 159398. [CrossRef]

22. Ganshina, E.A.; Garshin, V.V.; Pripechenkov, I.M.; Ivkov, S.A.; Sitnikov, A.V.; Domashevskaya, E.P. Effect of phase transformations of a metal component on the magneto-optical properties of thin-films nanocomposites $(CoFeZr)_x(MgF_2)_{100-x}$. *Nanomaterials* **2021**, *11*, 1666. [CrossRef] [PubMed]

23. Kalinin, Y.E.; Sitnikov, A.V.; Stognei, O.V.; Zolotukhin, I.V. Electrical properties and giant magnetoresistance of the CoFe–SiO_2 amorphous granular composites. *Mater. Sci. Eng. A* **2001**, *304*, 941–945. [CrossRef]

24. Stogneĭ, O.V.; Sitnikov, A.V.; Kalinin, Y.E.; Avdeev, S.F.; Kopytin, M.N. Isotropic positive magnetoresistance in Co-Al_2O_n nanocomposites. *Phys. Solid State* **2007**, *49*, 164–170. [CrossRef]

25. Nikiruy, K.E.; Iliasov, A.I.; Emelyanov, A.V.; Sitnikov, A.V.; Rylkov, V.V.E.; Demin, V.A. Memristors Based on Nanoscale Layers $LiNbO_3$ and $(Co_{40}Fe_{40}B_{20}) \times (LiNbO_3)$ 100–*x*. *Phys. Solid State* **2020**, *62*, 1732–1735. [CrossRef]

26. Nikiruy, K.E.; Emelyanov, A.V.; Demin, V.A.; Sitnikov, A.V. Dopamine-like STDP modulation in nanocomposite memristors. *AIP Adv.* **2019**, *9*, 065116. [CrossRef]

27. Kijima-Aoki, H.; Cao, Y.; Kobayashi, N.; Takahashi, S. Large magnetodielectric effect based on spin-dependent charge transfer in metal-insulator type Co-(BaF_2) nanogranular films. *J. Appl. Phys.* **2020**, *128*, 133904. [CrossRef]

28. Cao, Y.; Kobayashi, N.; Zhang, Y.W.; Ohnuma, S.; Masumoto, H. Enhanced spin-dependent charge transport of Co-(Al-fluoride) granular nanocomposite by co-separate sputtering. *J. Appl. Phys.* **2017**, *122*, 1–7. [CrossRef]

29. Mitani, S.; Fujimori, H.; Ohnuma, S. Spin-dependent tunneling phenomena in insulating granular systems. *J. Magn. Magn. Mater.* **1997**, *165*, 141–148. [CrossRef]

30. Moodera, J.S.; Mathon, G. Spin polarized tunneling in ferromagnetic junctions. *J. Magn. Magn. Mater.* **1999**, *200*, 248–273. [CrossRef]

31. Barsoukov, E.E.; Macdonald, J.R. *Impedance Spectroscopy: Theory, Experiment, and Applications*; Willey: New York, NY, USA, 2005; p. 606. [CrossRef]

32. Poklonsky, N.A.; Gorbachuk, N.I. *Fundamentals of Impedance Spectroscopy of Composites: A Course of Lectures*; Belaruce State University: Minsk, Belarus, 2005; p. 130.

33. Koltunowicz, T.N.; Zukowski, P.; Boiko, O.; Czarnacka, K. Capacitive properties of nanocomposite $(FeCoZr)_x(PZT)(100-x)$ produced by sputtering with the use of argon and oxygen ions beam. *J. Mater. Sci. Mater. Electron.* **2016**, *27*, 1171–1176. [CrossRef]